

Evaluating Text-to-Image and Text-to-Video Synthesis with a Conditional Fréchet Distance

Jaywon Koo*, Jefferson Hernandez*, Moayed Haji-Ali, Ziyang Yang, and Vicente Ordonez
Rice University

{jk125, jefehern, mh155, zy47, vicenteor}@rice.edu

<https://github.com/JaywonKool7/cFreD>

Abstract

Evaluating text-to-image and text-to-video models is challenging due to a fundamental disconnect: established metrics fail to jointly measure visual quality and semantic alignment with text, leading to a poor correlation with human judgments. To address this critical issue, we propose cFreD, a general metric based on a Conditional Fréchet Distance that unifies the assessment of visual fidelity and text-prompt consistency into a single score. Existing metrics such as Fréchet Inception Distance (FID) capture image quality but ignore text conditioning while alignment scores such as CLIPScore are insensitive to visual quality. Furthermore, learned preference models require constant retraining and are unlikely to generalize to novel architectures or out-of-distribution prompts. Through extensive experiments across multiple recently proposed text-to-image models and diverse prompt datasets, cFreD exhibits a higher correlation with human judgments compared to statistical metrics, including metrics trained with human preferences. Our findings validate cFreD as a robust, future-proof metric for the systematic evaluation of text conditioned models, standardizing benchmarking in this rapidly evolving field. We release our evaluation toolkit and benchmark [here](#).

1. Introduction

Generative models have demonstrated remarkable capabilities in text-to-image generation [18, 25, 58, 63], text-to-video generation [6, 37, 40, 64, 68, 83], and other modalities [5, 26, 27, 29, 52, 87]. This progress has been driven by technical breakthroughs such as the development and improved understanding of Generative Adversarial Networks (GANs) [23], Variational AutoEncoders (VAEs) [34], and more recently models based on Denoising Diffusion [70] and Flow Matching [47]. Automatic evaluation metrics have played a crucial role in guiding the development and refine-

*Equal contribution.

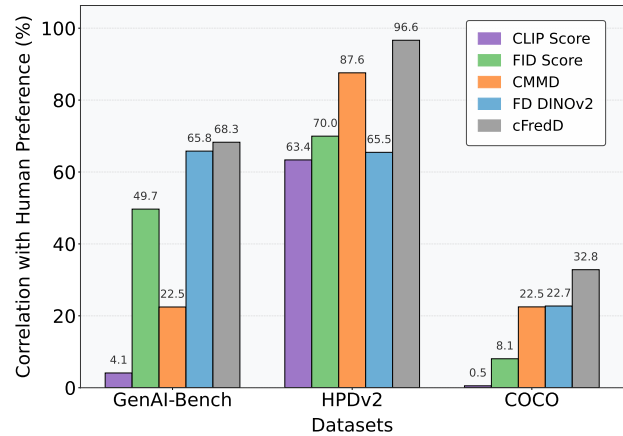


Figure 1. Correlation of five evaluation metrics with human preferences on three benchmark datasets (GenAI-Bench, HPDV2, and COCO). Compared to FID, FD_{DINOv2} , CLIPScore, and CMMD, our proposed method (cFreD) achieves consistently higher correlation with human judgments across all datasets.

ment of these models by offering quantitative benchmarks that compare the quality, diversity, and fidelity of various generative approaches. The most commonly used metrics include Inception Score (IS) [66], Fréchet Inception Distance (FID) [32], and CLIPScore [31].

We consider that it is time to reassess evaluation metrics for text-to-image synthesis and propose cFreD, based on a conditional formulation of Fréchet Distance. Prior work has reported that existing metrics exhibit weak correlation with human preferences [36, 51, 79, 81]. Additionally, metrics such as IS or FID, although indicative of image quality to some extent, do not measure the alignment of generated images with input text prompts, focusing solely on comparing the generated image distributions with respect to a reference set [4]. For instance, consider a dataset with two images: one of a *dog* and one of a *cat*, each paired with their corresponding prompt. A perfect text-to-image model that mistakenly swaps these mappings (*i.e.* generating a *cat* for *dog* prompt and vice versa) would achieve near zero FID since the overall

distribution of cats and dogs is maintained, despite the misalignment with the intended prompts. We show that cFreD captures better image quality assessment and conditioning on input text and results in improved correlation with human preferences (see Fig. 1 and Fig. 2). cFreD seamlessly extends to text-to-video generation, where it matches the best metric in correlation to human preferences on recent benchmarks, confirming that the same conditional formulation scales to the temporal domain. Moreover, we demonstrate that cFreD behaves monotonically under severe latent-space image corruptions and prompt perturbations, whereas traditional scores such as FID can be misleading, showcasing its robustness beyond the clean-data regime.

Currently, the most reliable form of evaluation for text-to-image models relies on collecting human preference data through crowd-sourcing, similar to the way Large Language Models (LLMs) are evaluated (i.e. the LMSys Arena [10]). For instance, the Parti Prompts Arena [54] employs 1,600 English prompts originally designed for assessing Parti models [84], presenting users with a gamified task of selecting their preferred image from two random outputs generated by four different models played over 10 rounds. Similarly, the Text-to-Image Arena Leaderboard [2] asks users to compare the outputs from two randomly selected models given a prompt, and their preferences are used to calculate *ELO* scores. However, collecting enough human preference data to statistically establish model superiority is time-intensive, and these arenas risk becoming unmaintained over time, as evidenced by the Parti Prompts Arena, which no longer collects votes. Recent work has also proposed learning metrics directly from human preferences [36, 78, 79, 81, 90]. However, it remains unclear whether such metrics trained on data from previous generative models can effectively assess the next generation of models. Moreover, since human preferences are inherently dynamic and evolve over time, these models risk becoming outdated unless they are regularly updated with fresh preference data. As a result, metrics such as FID, CLIPScore and our proposed cFreD will continue to play an important role in model evaluation.

Most related to our work is the previously proposed conditional Fréchet Inception Distance (cFID) by Soloveitchik et al. [71]. Unlike traditional statistical metrics, cFID incorporates a conditioning modality to evaluate not only visual quality but also alignment with respect to an input condition. We revisit and apply this formulation, originally proposed to evaluate image-to-image generation, to text-to-image generation. Furthermore, we systematically analyze how the choice of vision and text backbone models affect metric performance and demonstrate that the previously used Inception V3 [74] model is an outdated choice. By replacing it with a superior backbone model, we propose cFreD as a superior alternative to other statistical metrics (see Fig. 1).

Our contributions can be summarized as follows:

- We demonstrate that a metric based on Conditional Fréchet Distance (cFreD) is a powerful alternative to the more common practice of evaluating text-to-image models with a combination of FID and CLIPScore.
- We show that cFreD correlates strongly with human evaluations, outperforming prior statistical metrics on four text-to-image human preference datasets and matching the best metric on two text-to-video human preference datasets.
- We open-source our evaluation toolkit and offer the community a unified version of the Partiprompts Arena.

2. Related Work

Text-to-Image Generation Metrics. Text-to-image synthesis has progressed from early GANs [82, 86] to today’s diffusion and autoregressive models such as GLIDE, Imagen, and DALLE [53, 61, 65]. Quality is still commonly measured with Fréchet Inception Distance (FID) and Inception Score (IS) [32, 66], which emphasize image realism/diversity but correlate only loosely with human judgments and ignore text alignment [33]. To address this, CLIP-based metrics, including CLIPScore [31], CMMD [33], and FD_{DINOv2} [72], compare image–text pairs in a joint representation space, while alternatives such as FWD [76] (wavelet statistics) and perceptual LPIPS [88] target visual fidelity alone. Despite these refinements, existing scores still under-represent the nuanced trade-off between image quality and semantic faithfulness that guides human preference. Our proposed cFreD integrates the text prompt directly into the distance computation, producing evaluations that align more closely with human ratings of text-to-image outputs.

Text-to-Video Generation Metrics. Early work repurposed image-centric scores: Fréchet Video Distance (FVD) on I3D features captures visual realism but misses motion/text cues, whereas frame-wise CLIPScore [31] adds a text component yet remains motion blind. T2VBench introduces 16 controlled temporal scenarios that expose consistency failures, while EvalCrafter [50] uses 17 objective metrics to measure perceptual quality, motion, and text alignment. JEDi [51] replaces FVD’s Gaussian assumption with an MMD on JEPA embeddings, reducing sample needs, while learning-based evaluators such as VideoScore [30] align well with human judgments but demand expensive retraining, and don’t measure the alignment of the generative distribution beyond human preferences. In contrast, our cFreD simultaneously captures temporal and perceptual fidelity *and* text alignment without retraining.

Evaluating with Human Preferences. A complementary line of research replaces statistical metrics with direct human feedback, assembling large-scale preference datasets in which annotators pick or rank images for a given prompt [21, 36, 39, 56, 78, 79, 81, 89, 90]. Early efforts such as HPS [79] and PickScore [36] crowd-sourced $\sim 100k$ and

Prompt: "A living room with a couch and a laptop computer resting on the couch."



Figure 2. Comparison of image rankings across different evaluation metrics for the prompt ‘A living room with a couch and a laptop computer resting on the couch.’ Each row displays how images are ranked from 1 to 9 according to a specific metric (Human preference, FID, CLIP, CMMD, ImageReward, and cFreD), illustrating how different metrics prioritize distinct visual qualities. Inside a **green** box is the highest rated model as judged by human preferences (FLUX.1-dev) and inside a **purple** box is the lowest rated model as judged by human preferences (SDv1.5). cFreD is the only statistical metric that preserves their relative ordering.

~500k pairwise votes, respectively, then fine-tuned CLIP (L/14 or H/14) so that “preferred” images obtain higher image–text similarity. ImageReward [81] (137k pairs), HPSv2 [78] (108k GPT-cleaned prompts), and MPS [89] (66k multi-aspect rankings) further extend scale, data sanitation, and evaluation axes; training reward models that outperform FID/IS on human correlation. While these datasets improve alignment with user preferences, they demand expensive annotation and still entangle aesthetics, realism, and semantic faithfulness. Our work pursues a lighter-weight alternative: a metric that leverages textual context without

relying on human-preference supervision. Unlike preference-trained metrics, which may overfit to current model families seen during training and struggle with small synthetic (e.g., CIFAR-100) or domain-specific data (e.g., aerial or medical imaging), cFreD requires no extra training and offers a reliable plug-and-play solution across diverse settings.

3. Methodology

In this work, we evaluate text-to-image synthesis using a conditional variant of the Fréchet Distance (FD). This formulation was also proposed in the work of Soloveitchik et

Dataset	FID		FD _{DINOv2}		CLIP		CMMD		cFrED	
	ρ^2	Rank Acc.	ρ^2	Rank Acc.	ρ^2	Rank Acc.	ρ^2	Rank Acc.	ρ^2	Rank Acc.
HPDv2 [78]	0.70	86.7	0.65	86.7	0.63	15.6	0.88	80.0	0.97	91.1
Gen-AI Bench [46]	0.50	80.0	0.66	86.7	0.04	40.0	0.22	66.7	0.68	86.7
PartiPrompts [54]	0.70	-	0.70	-	0.12	-	0.54	-	0.73	-
COCO [45]	0.08	41.7	0.29	36.1	0.00	47.2	0.22	30.6	0.33	66.7
Avg.	0.50	69.5	0.58	69.8	0.20	34.3	0.47	59.1	0.68	81.5

Table 1. Correlation to human preference and rank accuracy of statistical metrics on four text-to-image datasets (HPDv2, Parti-Prompts, COCO and Gen-AI Bench). The best results are shown in **bold**. cFrED consistently achieves the highest correlation with human preference and rank accuracy across all four datasets.

al. [71] as a conditional version of the FID metric. For succinctness, we offer here a review of this formulation. Unlike the standard Fréchet Distance (FD) which only compares the marginal distributions of real and generated images, *conditional FD* accounts for the conditioning provided by a text prompt x .

3.1. Conditional Fréchet Distance

For a given prompt x , we assume that the real image y and the generated image \hat{y} are drawn from the conditional distributions

$$\begin{aligned} Q_{y|x} &= \mathcal{N}(\mu_{y|x}, \Sigma_{yy|x}), \\ Q_{\hat{y}|x} &= \mathcal{N}(\mu_{\hat{y}|x}, \Sigma_{\hat{y}\hat{y}|x}), \end{aligned} \quad (1)$$

where $\mu_{y|x}$ and $\mu_{\hat{y}|x}$ are the conditional means, and $\Sigma_{yy|x}$ and $\Sigma_{\hat{y}\hat{y}|x}$ are the conditional covariance matrices. These statistics capture the distribution of images corresponding to the text prompt.

Following the derivation in [71], the conditional Fréchet Distance is defined as the expectation over the prompts of the distance between the two conditional Gaussian distributions:

$$\begin{aligned} \text{cFrED} = \mathbb{E}_x \left[\left\| \mu_{y|x} - \mu_{\hat{y}|x} \right\|^2 \right. \\ \left. + \text{Tr} \left(\Sigma_{yy|x} + \Sigma_{\hat{y}\hat{y}|x} - 2 \left(\Sigma_{yy|x}^{1/2} \Sigma_{\hat{y}\hat{y}|x} \Sigma_{yy|x}^{1/2} \right)^{1/2} \right) \right]. \end{aligned}$$

An equivalent formulation can be derived that expresses cFrED in terms of the unconditional moments and the cross-covariances:

$$\begin{aligned} \text{cFrED} = \left\| \mu_y - \mu_{\hat{y}} \right\|^2 + \text{Tr} \left[\left(\Sigma_{yx} - \Sigma_{\hat{y}x} \right) \Sigma_{xx}^{-1} \left(\Sigma_{xy} - \Sigma_{x\hat{y}} \right) \right] \\ + \text{Tr} \left[\Sigma_{yy|x} + \Sigma_{\hat{y}\hat{y}|x} - 2 \left(\Sigma_{yy|x}^{1/2} \Sigma_{\hat{y}\hat{y}|x} \Sigma_{yy|x}^{1/2} \right)^{1/2} \right]. \end{aligned}$$

In these expressions, μ_y and $\mu_{\hat{y}}$ are the unconditional means of the real and generated images, respectively. In contrast, Σ_{yx} and $\Sigma_{x\hat{y}}$ denote the cross-covariances with the input prompt x .

By incorporating the prompt x , cFrED simultaneously measures (1) the realism of the generated images (via the comparison of unconditional statistics) and (2) the fidelity of the generated images with respect to the text prompt (via the conditional moments and cross-covariances). Thus, cFrED provides a more comprehensive evaluation metric for text-to-image models compared to traditional FID, which may fail to penalize cases where a model produces realistic images that are uncorrelated with the input prompt.

4. Experiment Settings

In this section, we introduce the experimental setup and report the results on two tasks. We next compare it with preference-trained metrics, variants of cFrED using different backbones, and the FID + CLIPScore combination.

4.1. Experimental Setup

Dataset. To evaluate how correlated our metric is with human preferences, we need rankings of generated images from different models using the same prompt. We use three different datasets (HPDv2 [78], Gen-AI Bench [46], and PartiPrompts [54]), which contain different generated images (each from a different model) for each prompt, along with the human preferences. We took the most preferred image per prompt as the reference image, since the real image was not always rated highest by humans. To evaluate recent models, we randomly selected 1,000 prompts from the COCO train and validation sets, ensuring these prompts were not part of the HPDv2 training and testing sets. For each prompt, we generated images using nine models listed on the Arena Leaderboard [2]. The original COCO images serve as reference images in this evaluation.

Metric Comparison & Evaluation Setting. We compare cFrED against four statistical metrics (FID [32], FD_{DINOv2} [72], CLIPScore [31], and CMMD [33]). For text-to-video, we also compare with four statistical metrics (FVD [75], JEDi [51], Inception Score, and CLIPScore). We evaluate human correlation ρ for scoring perspectives and calculate the Rank Accuracy to compare ranks. cFrED uses

Dataset	FVD		JEDi		IS		CLIP		cFreD	
	ρ^2	Rank Acc.	ρ^2	Rank Acc.	ρ^2	Rank Acc.	ρ^2	Rank Acc.	ρ^2	Rank Acc.
T2VQA-DB [38]	0.82	86.7	0.69	82.2	0.59	73.3	0.01	57.8	0.86	91.1
EvalCrafter [50]	0.93	80.0	0.60	20.0	0.79	80.0	0.46	40.0	0.90	100
Avg.	0.88	83.35	0.65	51.1	0.69	76.7	0.24	48.9	0.88	95.6

Table 2. Correlation to human preference and rank accuracy of statistical metrics on two text-to-video datasets (T2VQA-DB and EvalCrafter). The best results are shown in **bold**. cFreD achieves the highest average correlation and rank accuracy with two datasets, demonstrating strong alignment with human judgement in text-to-video evaluation.

DINOv2-G/14¹ for image embedding and the OpenCLIP ConvNext-B Text Encoder² for text embeddings. For text-to-video, cFreD uses for text embedding and FVD’s I3D for video embeddings.

Rank Accuracy. This metric quantifies the proportion of correctly ordered pairs—that is, it represents the probability that a randomly selected pair is concordant with the true rank. Previous works on learning human preferences [67, 78, 81, 89] measure performance using per item rank accuracy, which computes the ranking accuracy for each image-text pair and then averages the results. In contrast, cFreD evaluates the overall ranking performance across the entire dataset by computing a global rank accuracy. For statistical metrics [31–33, 72], we follow this convention and derive rankings directly from their raw scores. For human preference-trained metrics, we first average the ranking each model receives over all samples and then determine the final ranking based on these averages.

4.2. Results on Text-to-Image

As shown in Table 1, cFreD achieves the highest correlation with human preference and the highest rank accuracy among all statistical metrics across the four benchmarks. FID and FD_{DINOv2} show only moderate alignment, while the CLIP score performs poorly and CMMD provides only marginal improvements. In contrast, cFreD consistently outperforms all baselines, achieving the highest correlation and ranking accuracy on every dataset. We provide full per-dataset breakdowns in the supplementary material. These results suggest that cFreD provides a significantly more reliable and generalizable metric for human perceptual evaluation in text-to-image generation tasks.

Fig. 2 shows how different evaluation metrics (FID, CLIP, CMMD, ImageReward, and cFreD) rank the same set of images from best to worst for the prompt, with human preferences highlighting the best (green box) and worst (purple box) outputs. Notably, cFreD is the only statistical metric that preserves the human-chosen ordering.

¹[timm/vit-giant_patch14_dinov2.lvd142m](https://github.com/timm/vit-giant_patch14_dinov2.lvd142m)

²[convnext_base_w_laion2b_s13b_b82k_augreg](https://github.com/facebookresearch/convnext_base_w_laion2b_s13b_b82k_augreg)

4.3. Results on Text-to-Video

Tab. 2 shows the comparison of cFreD with four other text-to-video statistical metrics across two benchmarks: T2VQA-DB [38] and EvalCrafter [50]. cFreD consistently achieves the highest rank accuracy and among the highest correlations with human preference across both datasets. While FVD performs strongly in terms of correlation (avg. $\rho^2 = 0.88$), its rank accuracy is notably lower at 83.35%. Other baselines, such as JEDi, IS, and CLIP, perform worse. These results highlight the robustness and generalizability of cFreD, demonstrating its closer alignment with human judgement in text-to-video evaluation.

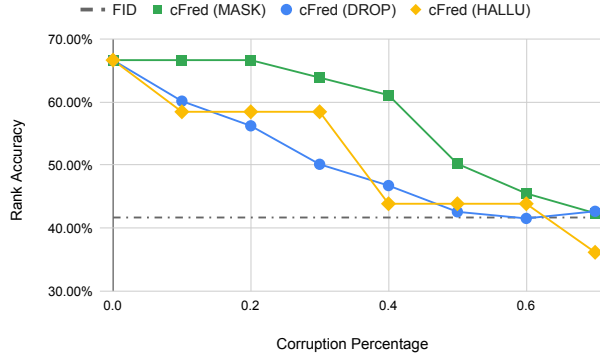
4.4. Are we done with FID?

FID and CLIPScore have been the main metrics for evaluating text-to-image synthesis. We performed an extra experiment where we explored a linear combination of these two metrics optimized on the COCO dataset. Although this combined metric achieved a non-trivial rank accuracy of 60%, its performance still lagged behind that of cFreD. More critically, when applied to the HPDv2 dataset, the combined metric’s rank accuracy lowered to 30%—worse than using FID or CLIPScore individually.

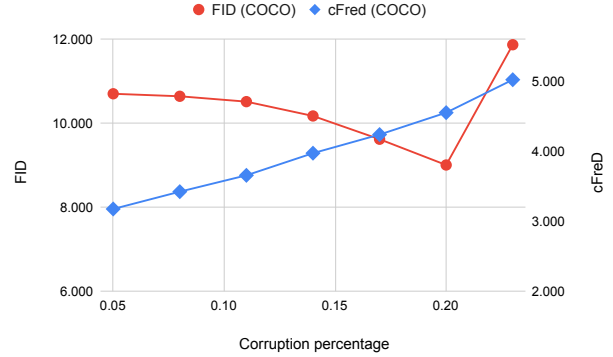
These results not only question the utility of combining FID and CLIPScore, but also highlight the inherent limitations of FID in capturing the text–image alignment necessary for the evaluation of text-to-image generation. Based on our experiments on PartiPrompts, HPDv2, and COCO, we argue that researchers should shift their focus towards monitoring cFreD and CLIPScore as the primary evaluation metrics.

4.5. Are we done with InceptionV3?

For this experiment, we include InceptionV3 as one of the backbones for cFreD. Our experimental results, summarized in Fig. 4, show a head-to-head comparison of each image backbone’s ranking of the diffusion models against the ground-truth ranking, reported as a “win rate”. Specifically, for each backbone, we measure how often its ranking of the diffusion models agrees with the actual human-derived ordering (win), disagrees (lose), or ties (split into both good or both bad). Although InceptionV3 still secures a portion of wins, it lags behind newer transformer-based backbones,



(a) **Robustness of text distortions.** We progressively corrupt the caption embeddings by (i) replacing random tokens with [MASK] (MASK), (ii) randomly dropping tokens (DROP), or (iii) hallucinating new tokens with an external LLM (HALLU).



(b) **Robustness of image distortions.** Images are first encoded with a VQ-VAE; we then progressively add uniform noise to a growing fraction of latent codes before decoding. Here cFreD rises monotonically with corruption, faithfully tracking visual degradation.

Figure 3. **Robustness study on the COCO.** dataset We inject noise either into the *text* branch (a) or the *image* branch (b) and compare cFreD with the conventional FID baseline. Across both settings, cFreD responds consistently to quality degradation, whereas FID can be insensitive (a) or misleading (b).

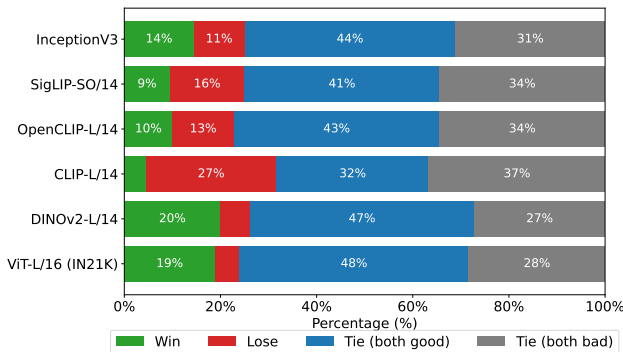


Figure 4. **Win rates** between the concordance of the true rank against the ranking created by each image backbone when evaluated on the COCO dataset.

such as DINOv2-L/14 and ViT-L/16, which consistently achieve higher win rates and fewer mismatches. These findings suggest that, although InceptionV3 remains a good baseline, more advanced architectures yield rankings that better align with human judgment on the COCO dataset, reinforcing the move away from InceptionV3 in state-of-the-art text-to-image evaluations.

4.6. Comparison with Human Preference Trained Metrics

Tab. 3 compares cFreD with existing metrics trained on human preference across text-to-image and text-to-video evaluation settings. In the text-to-image domain (Table 3a), cFreD consistently achieves the highest correlation and rank accuracy on HPDv2 and remains competitive on Gen-AI Bench, despite not using any human preference-based training. In the text-to-video domain (Table 3b), cFreD

(a) Text-to-Image Evaluation								
Dataset	HPSv2		MPS		VQAScore		cFreD	
	ρ^2	Rank Acc.	ρ^2	Rank Acc.	ρ^2	Rank Acc.	ρ^2	Rank Acc.
HPDv2 [79]	0.90	88.9	0.86	86.7	0.62	80.0	0.97	91.1
Gen-AI Bench [46]	0.79	87.7	0.45	73.3	0.99	93.3	0.68	86.7

(b) Text-to-Video Evaluation							
Dataset	VideoScore 1.1		VisionReward		cFreD		
	ρ^2	Rank Acc.	ρ^2	Rank Acc.	ρ^2	Rank Acc.	
T2VQA-DB [38]	0.02	55.6	0.01	46.67	0.86	91.1	
EvalCrafter [50]	0.91	20.0	0.27	60.0	0.90	100.0	

Table 3. Comparison of cFreD (cFreD) with metrics trained using human preference across (a) text-to-image and (b) text-to-video evaluation settings. We report squared Spearman correlation (ρ^2) and rank accuracy (%) with human preference. Best results are shown in **bold**.

outperforms all preference-trained metrics on T2VQA-DB and achieves perfect rank accuracy on EvalCrafter, despite not using any human preference training. Notably, while VideoScore [30] achieves a slightly higher correlation on EvalCrafter ($\rho^2 = 0.91$), its rank accuracy drops to 20.0%, underscoring a gap between correlation and true preference alignment. These results highlight the generality and robustness of cFreD across two tasks. Unlike metrics trained on preference data, cFreD requires no re-training and can be readily applied to specialized domains such as medical or satellite images without any human annotation or domain-specific adaptation.

5. Ablations

To disentangle how image and text encoders influence cFreD, we exhaustively evaluated all combinations of vision and

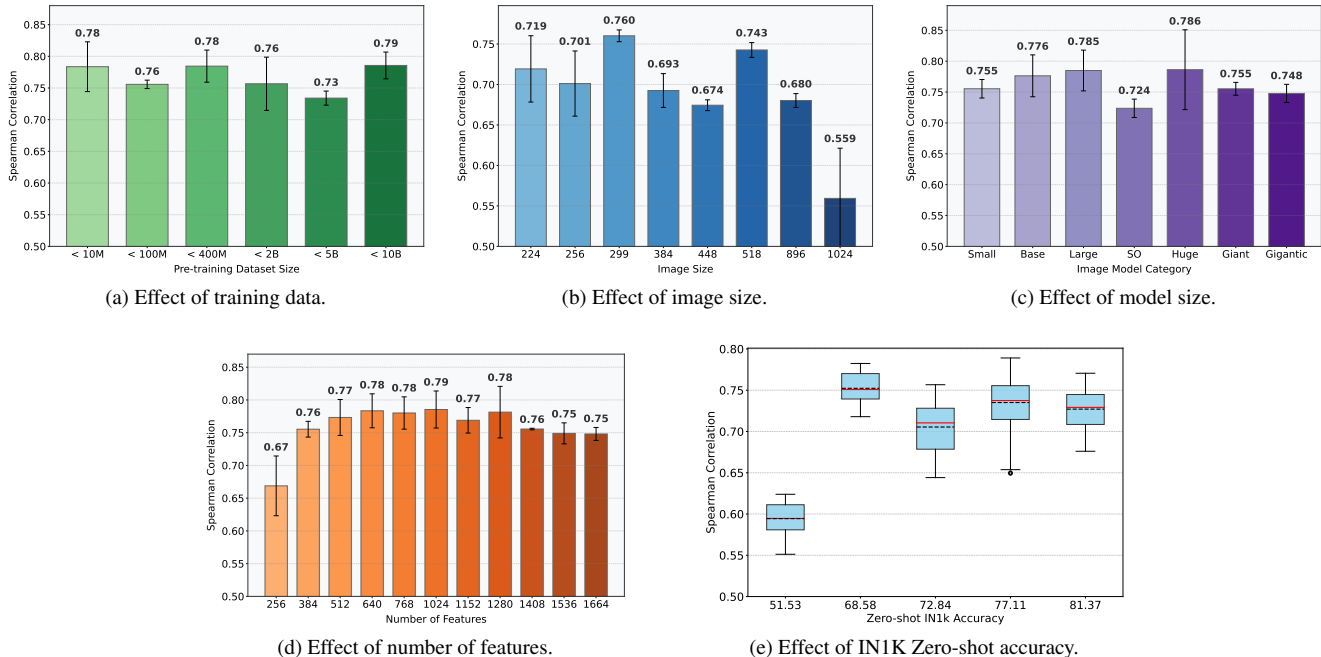


Figure 5. **Ablation study on the Parti-Prompts** dataset comparing the correlation to human preferences under varying factors: (a) the ViT training dataset, (b) input image size, (c) model capacity, (d) the number of features in the last ViT layer, and (e) zero-shot accuracy on ImageNet-1K.

language backbones (full list in the Appendix). Ideally, *A/B* experiments require training identical architectures while varying a *single* factor to isolate causal effects most cleanly. However, re-training a model on a billion-scale image corpus for every factor would demand too many resources. Rather than reporting raw correlations bucketed by individual factors, we approximate a controlled “one-factor-at-a-time” experiment by fitting (i) a multiple linear regression ($R^2 = 0.56$; $N = 1804$) and (ii) a mixed-effects model with random intercepts for each image encoder. These models provide *partial-dependence* estimates that isolate the marginal impact of every visual attribute on cFreD’s Spearman correlation with human preferences while averaging over all text encoders. All analyses are performed on the PARTIPROMPTS Arena. Comprehensive statistical outputs—including Type-II ANOVA tables, variance-inflation factors, and diagnostic plots—are included in the Appendix.

Effect of the size of the pre-training dataset on cFreD.

Fig. 5a reports the *partial-dependence* of cFreD on dataset size after controlling all other covariates. Models trained on >10 B images set the performance ceiling: the mixed-effects fit predicts 0.04–0.10 higher Spearman ρ than every smaller bucket (Type-II ANOVA $F=206$, $p < 10^{-170}$). All sub-billion regimes have sizable drops, with the 10M-image bucket suffering the largest penalty (-0.102 OLS; -0.077 mixed). Once these controlled effects are considered, the seemingly “strong” 10M result in the raw plot disappears and the relation between data scale and alignment becomes

monotonic. These findings confirm that sheer scale, rather than subtle confounds such as architecture or resolution, remains the single most powerful driver of cFreD’s agreement with human judgments, underscoring the value of massive and well-curated corpora for text-conditioned image generation metrics.

Effect of image size on cFreD. Fig. 5b plots the *partial-dependence* of cFreD on input crop size (shortest side, in pixels) after controlling for data scale, parameter counts, and feature width. The controlled effect is sharply negative: $\beta = -2.0 \times 10^{-4}$ Spearman ρ per pixel (OLS $t = -29$, $p < 10^{-100}$; mixed-effects $z = -4.3$, $p < 10^{-4}$), and Type-II ANOVA tags image size as a major factor ($F=860$, $p < 10^{-154}$). An increase in resolution from $224 \rightarrow 448$ is predicted to lower correlation by ≈ 0.045 ; this holds even larger inputs (e.g., ≥ 896), incurring steeper penalties. Moderate resolutions remain competitive—Inception-scale crops land near the peak; and the DINOv2 518 px setting lies on the declining slope. Apparent non-monotonicities in the raw means largely vanish once covariates are held fixed, suggesting that oversized crops dilute semantically salient regions relative to their captions (higher resolution images would need more detailed captions), degrading alignment with human judgments.

Effect of ViT model size on cFreD. Fig. 5c plots the *partial-dependence* of cFreD on image-encoder parameter count (log scale). Controlling for data scale, crop size, and feature width reverses the naive trend: each $10\times$ increase in param-

ters *decreases* Spearman ρ by 1.8 points (OLS $\beta = -0.018$, $t = -8.0$, $p = 2 \times 10^{-15}$) and by 2.6 points in the mixed model ($z = -2.5$, $p = 0.011$). Type-II ANOVA corroborates the effect ($F=64$, $p < 10^{-14}$). Hence, once confounds are removed, oversized ViT backbones offer no benefit, and can even hurt, alignment with human preferences, suggesting that additional capacity is unnecessary for cFreD.

Effect of ViT Feature dimensionality on cFreD. Fig. 5d shows the *partial-dependence* of cFreD on ViT embedding dimensionality. After controlling for data scale, crop size, and parameter count, each additional +100 channels boosts Spearman ρ by only +0.0025 (OLS $\beta = 2.5 \times 10^{-5}$, $t = 5.1$, $p = 3.6 \times 10^{-7}$; mixed $z = 17.4$, $p < 10^{-15}$). Gains taper beyond ~ 1 k dims but never reverse, contrary to the apparent high-dimensional downturn in the raw plot. Widths in the 1, 024–1, 280 range maximize correlation, yet leaner heads (512–640 dims) lag by barely < 0.01 . Thus, modest widening is beneficial, but very large feature spaces deliver only marginal improvements relative to their computational cost.

Effect of Zero-Shot ImageNet Accuracy on cFreD. Fig. 5e shows a boxplot of the correlation between cFreD and human preferences as a function of zero-shot ImageNet accuracy, evaluated exclusively on image-text pretrained models [19, 22, 59, 67, 80]. Higher zero-shot accuracies generally correspond to stronger correlations with human judgments, though variance exists within each accuracy level. Models with the highest accuracy (81.37%) achieve the highest median correlation, while models at the lower end (51.53%) cluster around lower correlation values. These findings suggest that zero-shot ImageNet performance can serve as a useful indicator of downstream alignment with human preferences despite considerable variability among models with similar accuracy levels.

5.1. Resilience to distortions

Here, we provide additional evidence that FID detects failures of image-text alignment under *complex* perturbations. For reference, it was shown in [32] that FID accurately captures image distortions under low-level image processing distortions such as Gaussian noise and Gaussian blur. Since cFreD is a generalization of FID, it also inherits this resilience to such distortions. Therefore, we instead focus on two harder stress tests: (i) disrupting the *image* in latent space and (ii) disrupting the *text* conditioning signal.

Image distortions. We follow the same setting as [74] and first encode every generated image with the pretrained Cosmos tokenizer [1], randomly replace a fixed fraction of latent tokens with codes uniformly sampled from the same codebook, and then decode the corrupted latents back. This procedure preserves the global colour statistics of the training data while progressively scrambling high-level structure. As shown in Fig. 3b, cFreD *monotonically increases* with

the corruption ratio, faithfully mirroring the visual degradation. In contrast, FID *decreases* between 5–20% corruption, suggesting that the images have *improved*, before shooting up once the latent codes become overwhelmingly noisy. The non-monotonic behaviour arises because replacing a moderate number of latents can accidentally move samples *closer* to the marginal distribution of the real data, something FID cannot disambiguate without joint image–text statistics. cFreD, by cross-checking against captions, correctly penalises the emerging misalignment at every corruption level. **Text distortions.** We corrupt captions fed to the text encoder while keeping images fixed, using three ways: (i) MASK: random token masking; (ii) DROP: random token deletion; and (iii) HALLU: hallucinating a portion of the caption using (LLaMA-3.1-70B-instruct [16]). The trends (Fig. 3a) reveal three regimes. *Low corruption:* cFreD remains well above the constant FID baseline, signalling correct alignment. *Medium corruption:* for MASK and DROP, the curves drift steadily downward and converge to FID, exactly as predicted by our formulation. When the text embeddings become noisy, the cross-covariance term averages out and cFreD collapses to the image-only score. *Hallucination:* hallucinated captions drive cFreD *below* FID, indicating anti-alignment between the fabricated text and the true image content. Throughout, FID fails to detect, as it only sees unchanged pixels.

6. Discussion and Conclusion

In this work, we extend and repurpose Conditional Fréchet Inception Distance (cFID), first introduced in [71], for text-to-image and text-to-video evaluation by replacing outdated backbones (InceptionV3) with modern vision and text encoders. Our analysis shows that transformer-based encoders (e.g., ViT, DINOv2, CLIP) align significantly better with human preferences. Building on this, we introduce cFreD, which captures semantic consistency between text and image, unlike FID or IS, and achieves higher correlation with human judgments. Our ablation further shows that performance depends on balancing model complexity, data diversity, and representation quality, not scaling the model or dataset. We advocate cFreD as a robust, plug-and-play metric requiring no annotations or training. By open-sourcing our implementation, we aim to promote more systematic evaluations and accelerate generative model research.

cFreD also offers a promising extension. cFreD can incorporate human preference-trained models’ encoders as backbones for hybrid evaluation, which leverages cFreD’s robust semantic alignment and human preference data’s fine-grained insights. It can also be adapted to other conditional tasks like image captioning or audio-to-video generation. Furthermore, cFreD can be generalized to evaluating multi-conditional models, such as ControlNet [87], making it broadly applicable across generative tasks.

References

- [1] Niket Agarwal, Arslan Ali, Maciej Bala, Yogesh Balaji, Erik Barker, Tiffany Cai, Prithvijit Chattopadhyay, Yongxin Chen, Yin Cui, Yifan Ding, et al. Cosmos world foundation model platform for physical ai. *arXiv preprint arXiv:2501.03575*, 2025. 8
- [2] Artificial Analysis. Text to image model arena. <https://artificialanalysis.ai/text-to-image/arena?tab=Leaderboard>. Accessed: March 02, 2025. 2, 4
- [3] Mahmoud Assran, Quentin Duval, Ishan Misra, Piotr Bojanowski, Pascal Vincent, Michael Rabbat, Yann LeCun, and Nicolas Ballas. Self-supervised learning from images with a joint-embedding predictive architecture. In *Proceedings of the IEEE/CVF Conference on Computer Vision and Pattern Recognition*, pages 15619–15629, 2023. 12
- [4] Stella Biderman. Conditional fr chet inception distance. <https://x.com/BlancheMinerva/status/1757206462806343991>. Accessed: March 04, 2025. 1
- [5] Tim Brooks, Aleksander Holynski, and Alexei A Efros. Instructpix2pix: Learning to follow image editing instructions. In *Proceedings of the IEEE/CVF conference on computer vision and pattern recognition*, pages 18392–18402, 2023. 1
- [6] Tim Brooks, Bill Peebles, Connor Holmes, Will DePue, Yufei Guo, Li Jing, David Schnurr, Joe Taylor, Troy Luhman, Eric Luhman, Clarence Ng, Ricky Wang, and Aditya Ramesh. Video generation models as world simulators. 2024. 1
- [7] Xinlei Chen, Saining Xie, and Kaiming He. An empirical study of training self-supervised vision transformers. In *Proceedings of the IEEE/CVF international conference on computer vision*, pages 9640–9649, 2021. 12
- [8] Xiaokang Chen, Zhiyu Wu, Xingchao Liu, Zizheng Pan, Wen Liu, Zhenda Xie, Xingkai Yu, and Chong Ruan. Janus-pro: Unified multimodal understanding and generation with data and model scaling. *arXiv preprint arXiv:2501.17811*, 2025. 14
- [9] Mehdi Cherti, Romain Beaumont, Ross Wightman, Mitchell Wortsman, Gabriel Ilharco, Cade Gordon, Christoph Schuhmann, Ludwig Schmidt, and Jenia Jitsev. Reproducible scaling laws for contrastive language-image learning. In *Proceedings of the IEEE/CVF conference on computer vision and pattern recognition*, pages 2818–2829, 2023. 12
- [10] Wei-Lin Chiang, Lianmin Zheng, Ying Sheng, Anastasios Nikolas Angelopoulos, Tianle Li, Dacheng Li, Hao Zhang, Banghua Zhu, Michael Jordan, Joseph E. Gonzalez, and Ion Stoica. Chatbot arena: An open platform for evaluating llms by human preference, 2024. 2
- [11] Hyung Won Chung, Le Hou, Shayne Longpre, Barret Zoph, Yi Tay, William Fedus, Yunxuan Li, Xuezhi Wang, Mostafa Dehghani, Siddhartha Brahma, et al. Scaling instruction-finetuned language models. *Journal of Machine Learning Research*, 25(70):1–53, 2024. 13
- [12] Alexis Conneau, Kartikay Khandelwal, Naman Goyal, Vishrav Chaudhary, Guillaume Wenzek, Francisco Guzm n, Edouard Grave, Myle Ott, Luke Zettlemoyer, and Veselin Stoyanov. Unsupervised cross-lingual representation learning at scale. *arXiv preprint arXiv:1911.02116*, 2019. 12
- [13] Jacob Devlin, Ming-Wei Chang, Kenton Lee, and Kristina Toutanova. Bert: Pre-training of deep bidirectional transformers for language understanding. In *Proceedings of the 2019 conference of the North American chapter of the association for computational linguistics: human language technologies, volume 1 (long and short papers)*, pages 4171–4186, 2019. 12
- [14] Ming Ding, Wendi Zheng, Wenyi Hong, and Jie Tang. Cogview2: Faster and better text-to-image generation via hierarchical transformers. *Advances in Neural Information Processing Systems*, 35:16890–16902, 2022. 13
- [15] Alexey Dosovitskiy, Lucas Beyer, Alexander Kolesnikov, Dirk Weissenborn, Xiaohua Zhai, Thomas Unterthiner, Mostafa Dehghani, Matthias Minderer, Georg Heigold, Sylvain Gelly, et al. An image is worth 16x16 words: Transformers for image recognition at scale. *arXiv preprint arXiv:2010.11929*, 2020. 12
- [16] Abhimanyu Dubey, Abhinav Jauhri, Abhinav Pandey, Abhishek Kadian, Ahmad Al-Dahle, Aiesha Letman, Akhil Mathur, Alan Schelten, Amy Yang, Angela Fan, et al. The llama 3 herd of models. *arXiv e-prints*, pages arXiv–2407, 2024. 8
- [17] Patrick Esser, Robin Rombach, and Bjorn Ommer. Taming transformers for high-resolution image synthesis. In *Proceedings of the IEEE/CVF conference on computer vision and pattern recognition*, pages 12873–12883, 2021. 13
- [18] Patrick Esser, Sumith Kulal, Andreas Blattmann, Rahim Entezari, Jonas M ller, Harry Saini, Yam Levi, Dominik Lorenz, Axel Sauer, Frederic Boesel, et al. Scaling rectified flow transformers for high-resolution image synthesis. In *Forty-first international conference on machine learning*, 2024. 1, 14
- [19] Alex Fang, Albin Madappally Jose, Amit Jain, Ludwig Schmidt, Alexander Toshev, and Vaishaal Shankar. Data filtering networks. *arXiv preprint arXiv:2309.17425*, 2023. 8, 12
- [20] Yuxin Fang, Wen Wang, Binhui Xie, Quan Sun, Ledell Wu, Xinggang Wang, Tiejun Huang, Xinlong Wang, and Yue Cao. Eva: Exploring the limits of masked visual representation learning at scale. In *Proceedings of the IEEE/CVF conference on computer vision and pattern recognition*, pages 19358–19369, 2023. 12
- [21] Stephanie Fu, Netanel Tamir, Shobhita Sundaram, Lucy Chai, Richard Zhang, Tali Dekel, and Phillip Isola. Dreamsim: Learning new dimensions of human visual similarity using synthetic data. *arXiv preprint arXiv:2306.09344*, 2023. 2
- [22] Samir Yitzhak Gadre, Gabriel Ilharco, Alex Fang, Jonathan Hayase, Georgios Smyrnis, Thao Nguyen, Ryan Marten, Mitchell Wortsman, Dhruva Ghosh, Jieyu Zhang, et al. Datacomp: In search of the next generation of multimodal datasets. *Advances in Neural Information Processing Systems*, 36: 27092–27112, 2023. 8, 12
- [23] Ian Goodfellow, Jean Pouget-Abadie, Mehdi Mirza, Bing Xu, David Warde-Farley, Sherjil Ozair, Aaron Courville, and Yoshua Bengio. Generative adversarial nets. In *Advances in Neural Information Processing Systems*. Curran Associates, Inc., 2014. 1
- [24] Shuyang Gu, Dong Chen, Jianmin Bao, Fang Wen, Bo Zhang, Dongdong Chen, Lu Yuan, and Baining Guo. Vector quan-

- tized diffusion model for text-to-image synthesis. In *Proceedings of the IEEE/CVF conference on computer vision and pattern recognition*, pages 10696–10706, 2022. 13
- [25] Moayed Haji-Ali, Guha Balakrishnan, and Vicente Ordonez. Elasticdiffusion: Training-free arbitrary size image generation through global-local content separation. In *Proceedings of the IEEE/CVF Conference on Computer Vision and Pattern Recognition*, pages 6603–6612, 2024. 1
- [26] Moayed Haji-Ali, Willi Menapace, Aliaksandr Siarohin, Guha Balakrishnan, Sergey Tulyakov, and Vicente Ordonez. Taming data and transformers for audio generation. *arXiv preprint arXiv:2406.19388*, 2024. 1
- [27] Moayed Haji-Ali, Willi Menapace, Aliaksandr Siarohin, Ivan Skorokhodov, Alper Canberk, Kwot Sin Lee, Vicente Ordonez, and Sergey Tulyakov. Av-link: Temporally-aligned diffusion features for cross-modal audio-video generation. *arXiv preprint arXiv:2412.15191*, 2024. 1
- [28] Kaiming He, Xinlei Chen, Saining Xie, Yanghao Li, Piotr Dollár, and Ross Girshick. Masked autoencoders are scalable vision learners. In *Proceedings of the IEEE/CVF conference on computer vision and pattern recognition*, pages 16000–16009, 2022. 12
- [29] Sen He, Wentong Liao, Michael Ying Yang, Yongxin Yang, Yi-Zhe Song, Bodo Rosenhahn, and Tao Xiang. Context-aware layout to image generation with enhanced object appearance. In *Proceedings of the IEEE/CVF conference on computer vision and pattern recognition*, pages 15049–15058, 2021. 1
- [30] Xuan He, Dongfu Jiang, Ge Zhang, Max Ku, Achint Soni, Sherman Siu, Haonan Chen, Abhranil Chandra, Ziyang Jiang, Aaran Arulraj, et al. Videoscore: Building automatic metrics to simulate fine-grained human feedback for video generation. *arXiv preprint arXiv:2406.15252*, 2024. 2, 6
- [31] Jack Hessel, Ari Holtzman, Maxwell Forbes, Ronan Le Bras, and Yejin Choi. Clipscore: A reference-free evaluation metric for image captioning. *arXiv preprint arXiv:2104.08718*, 2021. 1, 2, 4, 5
- [32] Martin Heusel, Hubert Ramsauer, Thomas Unterthiner, Bernhard Nessler, and Sepp Hochreiter. Gans trained by a two time-scale update rule converge to a local nash equilibrium. *Advances in neural information processing systems*, 30, 2017. 1, 2, 4, 8
- [33] Sadeep Jayasumana, Srikumar Ramalingam, Andreas Veit, Daniel Glasner, Ayan Chakrabarti, and Sanjiv Kumar. Rethinking fid: Towards a better evaluation metric for image generation. In *Proceedings of the IEEE/CVF Conference on Computer Vision and Pattern Recognition*, pages 9307–9315, 2024. 2, 4, 5
- [34] Diederik P. Kingma and Max Welling. Auto-encoding variational bayes. *International Conference on Learning Representations (ICLR)*, 2014. 1
- [35] Alexander Kirillov, Eric Mintun, Nikhila Ravi, Hanzi Mao, Chloe Rolland, Laura Gustafson, Tete Xiao, Spencer Whitehead, Alexander C Berg, Wan-Yen Lo, et al. Segment anything. In *Proceedings of the IEEE/CVF international conference on computer vision*, pages 4015–4026, 2023. 12
- [36] Yuval Kirstain, Adam Polyak, Uriel Singer, Shahbuland Matiana, Joe Penna, and Omer Levy. Pick-a-pic: An open dataset of user preferences for text-to-image generation. *Advances in Neural Information Processing Systems*, 36:36652–36663, 2023. 1, 2
- [37] Weijie Kong, Qi Tian, Zijian Zhang, Rox Min, Zuozhuo Dai, Jin Zhou, Jiangfeng Xiong, Xin Li, Bo Wu, Jianwei Zhang, et al. Hunyuanvideo: A systematic framework for large video generative models. *arXiv preprint arXiv:2412.03603*, 2024. 1
- [38] Tengchuan Kou, Xiaohong Liu, Zicheng Zhang, Chunyi Li, Haoning Wu, Xiongkuo Min, Guangtao Zhai, and Ning Liu. Subjective-aligned dataset and metric for text-to-video quality assessment. In *Proceedings of the 32nd ACM International Conference on Multimedia*, pages 7793–7802, 2024. 5, 6
- [39] Max Ku, Dongfu Jiang, Cong Wei, Xiang Yue, and Wenhui Chen. Viescore: Towards explainable metrics for conditional image synthesis evaluation. *arXiv preprint arXiv:2312.14867*, 2023. 2
- [40] Kuaishou. Kling video model. <https://kling.kuaishou.com/en>, 2024. 1
- [41] Black Forest Labs. Flux. <https://github.com/black-forest-labs/flux>, 2024. 14
- [42] Zhenzhong Lan, Mingda Chen, Sebastian Goodman, Kevin Gimpel, Piyush Sharma, and Radu Soricut. Albert: A lite bert for self-supervised learning of language representations. *arXiv preprint arXiv:1909.11942*, 2019. 12
- [43] Donghoon Lee, Jiseob Kim, Jisu Choi, Jongmin Kim, Minwoo Byeon, Woonhyuk Baek, and Saehoon Kim. Karlo-v1.0.alpha on coyo-100m and cc15m. <https://github.com/kakaobrain/karlo>, 2022. 13
- [44] Daiqing Li, Aleks Kamko, Ehsan Akhgari, Ali Sabet, Linmiao Xu, and Suhail Doshi. Playground v2.5: Three insights towards enhancing aesthetic quality in text-to-image generation, 2024. 14
- [45] Tsung-Yi Lin, Michael Maire, Serge Belongie, James Hays, Pietro Perona, Deva Ramanan, Piotr Dollár, and C Lawrence Zitnick. Microsoft coco: Common objects in context. In *Computer vision—ECCV 2014: 13th European conference, zurich, Switzerland, September 6–12, 2014, proceedings, part v 13*, pages 740–755. Springer, 2014. 4, 13
- [46] Zhiqiu Lin, Deepak Pathak, Baiqi Li, Jiayao Li, Xide Xia, Graham Neubig, Pengchuan Zhang, and Deva Ramanan. Evaluating text-to-visual generation with image-to-text generation. In *European Conference on Computer Vision*, pages 366–384. Springer, 2024. 4, 6
- [47] Yaron Lipman, Ricky T. Q. Chen, Heli Ben-Hamu, Maximilian Nickel, and Matthew Le. Flow matching for generative modeling. In *The Eleventh International Conference on Learning Representations*, 2023. 1
- [48] Xingchao Liu, Chengyue Gong, Lemeng Wu, Shujian Zhang, Hao Su, and Qiang Liu. Fusedream: Training-free text-to-image generation with improved clip+ gan space optimization. *arXiv preprint arXiv:2112.01573*, 2021. 13
- [49] Yinhan Liu, Myle Ott, Naman Goyal, Jingfei Du, Mandar Joshi, Danqi Chen, Omer Levy, Mike Lewis, Luke Zettlemoyer, and Veselin Stoyanov. Roberta: A robustly optimized bert pretraining approach. *arXiv preprint arXiv:1907.11692*, 2019. 12
- [50] Yaofang Liu, Xiaodong Cun, Xuebo Liu, Xintao Wang, Yong Zhang, Haoxin Chen, Yang Liu, Tiejong Zeng, Raymond

- Chan, and Ying Shan. Evalcrafter: Benchmarking and evaluating large video generation models. In *Proceedings of the IEEE/CVF Conference on Computer Vision and Pattern Recognition*, pages 22139–22149, 2024. 2, 5, 6
- [51] Ge Ya Luo, Gian Mario Faverio, Zhi Hao Luo, Alexia Jolicoeur-Martineau, and Christopher Pal. Beyond fvd: Enhanced evaluation metrics for video generation quality. *arXiv preprint arXiv:2410.05203*, 2024. 1, 2, 4
- [52] Sicheng Mo, Fangzhou Mu, Kuan Heng Lin, Yanli Liu, Bochen Guan, Yin Li, and Bolei Zhou. Freecontrol: Training-free spatial control of any text-to-image diffusion model with any condition. In *Proceedings of the IEEE/CVF Conference on Computer Vision and Pattern Recognition*, pages 7465–7475, 2024. 1
- [53] Alex Nichol, Prafulla Dhariwal, Aditya Ramesh, Pranav Shyam, Pamela Mishkin, Bob McGrew, Ilya Sutskever, and Mark Chen. Glide: Towards photorealistic image generation and editing with text-guided diffusion models. *arXiv preprint arXiv:2112.10741*, 2021. 2, 13
- [54] OpenGenAI. Parti prompts leaderboard. <https://huggingface.co/spaces/OpenGenAI/parti-prompts-leaderboard>. Hugging Face Space. Accessed: March 02, 2025. 2, 4
- [55] Maxime Oquab, Timothée Darcet, Théo Moutakanni, Huy Vo, Marc Szafraniec, Vasil Khalidov, Pierre Fernandez, Daniel Haziza, Francisco Massa, Alaaeldin El-Nouby, et al. Dinov2: Learning robust visual features without supervision. *arXiv preprint arXiv:2304.07193*, 2023. 12
- [56] Yang Peng, Yuxin Cui, Haomiao Tang, Zekun Qi, Runpei Dong, Jing Bai, Chunrui Han, Zheng Ge, Xiangyu Zhang, and Shu-Tao Xia. Dreambench++: A human-aligned benchmark for personalized image generation. *arXiv preprint arXiv:2406.16855*, 2024. 2
- [57] Pablo Pernias, Dominic Rampas, Mats Leon Richter, Christopher Pal, and Marc Aubreville. Würstchen: An efficient architecture for large-scale text-to-image diffusion models. In *The Twelfth International Conference on Learning Representations*, 2024. 13
- [58] Dustin Podell, Zion English, Kyle Lacey, Andreas Blattmann, Tim Dockhorn, Jonas Müller, Joe Penna, and Robin Rombach. Sdxl: Improving latent diffusion models for high-resolution image synthesis. *arXiv preprint arXiv:2307.01952*, 2023. 1, 13, 14
- [59] Alec Radford, Jong Wook Kim, Chris Hallacy, Aditya Ramesh, Gabriel Goh, Sandhini Agarwal, Girish Sastry, Amanda Askell, Pamela Mishkin, Jack Clark, et al. Learning transferable visual models from natural language supervision. In *International conference on machine learning*, pages 8748–8763. Pmlr, 2021. 8, 12, 15, 16
- [60] Colin Raffel, Noam Shazeer, Adam Roberts, Katherine Lee, Sharan Narang, Michael Matena, Yanqi Zhou, Wei Li, and Peter J Liu. Exploring the limits of transfer learning with a unified text-to-text transformer. *Journal of machine learning research*, 21(140):1–67, 2020. 13
- [61] Aditya Ramesh, Mikhail Pavlov, Gabriel Goh, Scott Gray, Chelsea Voss, Alec Radford, Mark Chen, and Ilya Sutskever. Zero-shot text-to-image generation. In *International conference on machine learning*, pages 8821–8831. Pmlr, 2021. 2
- [62] Aditya Ramesh, Prafulla Dhariwal, Alex Nichol, Casey Chu, and Mark Chen. Hierarchical text-conditional image generation with clip latents. *arXiv preprint arXiv:2204.06125*, 1(2): 3, 2022. 13
- [63] Robin Rombach, Andreas Blattmann, Dominik Lorenz, Patrick Esser, and Björn Ommer. High-resolution image synthesis with latent diffusion models. In *Proceedings of the IEEE/CVF conference on computer vision and pattern recognition*, pages 10684–10695, 2022. 1, 13, 14
- [64] RunwayML. Gen-3 alpha. <https://runwayml.com/research/introducing-gen-3-alpha>, 2024. 1
- [65] Chitwan Saharia, William Chan, Saurabh Saxena, Lala Li, Jay Whang, Emily L Denton, Kamyar Ghasemipour, Raphael Gontijo Lopes, Burcu Karagol Ayan, Tim Salimans, et al. Photorealistic text-to-image diffusion models with deep language understanding. *Advances in neural information processing systems*, 35:36479–36494, 2022. 2
- [66] Tim Salimans, Ian Goodfellow, Wojciech Zaremba, Vicki Cheung, Alec Radford, and Xi Chen. Improved techniques for training gans. *Advances in neural information processing systems*, 29, 2016. 1, 2
- [67] Christoph Schuhmann, Romain Beaumont, Richard Vencu, Cade Gordon, Ross Wightman, Mehdi Cherti, Theo Coombes, Aarush Katta, Clayton Mullis, Mitchell Wortsman, et al. Laion-5b: An open large-scale dataset for training next generation image-text models. *Advances in neural information processing systems*, 35:25278–25294, 2022. 5, 8, 12
- [68] Team Seaweed, Ceyuan Yang, Zhijie Lin, Yang Zhao, Shanchuan Lin, Zhibei Ma, Haoyuan Guo, Hao Chen, Lu Qi, Sen Wang, Feng Cheng, Feilong Zuo Xuejiao Zeng, Ziyang Yang, Fangyuan Kong, Zhiwu Qing, Fei Xiao, Meng Wei, Tuyen Hoang, Siyu Zhang, Peihao Zhu, Qi Zhao, Jiangqiao Yan, Liangke Gui, Sheng Bi, Jiashi Li, Yuxi Ren, Rui Wang, Huixia Li, Xuefeng Xiao, Shu Liu, Feng Ling, Heng Zhang, Houmin Wei, Huafeng Kuang, Jerry Duncan, Junda Zhang, Junru Zheng, Li Sun, Manlin Zhang, Renfei Sun, Xiaobin Zhuang, Xiaojie Li, Xin Xia, Xuyan Chi, Yanghua Peng, Yuping Wang, Yuxuan Wang, Zhongkai Zhao, Zhuo Chen, Zuquan Song, Zhenheng Yang, Jiashi Feng, Jianchao Yang, and Lu Jiang. Seaweed-7b: Cost-effective training of video generation foundation model, 2025. 1
- [69] Arseniy Shakhmatov, Anton Razzhigaev, Aleksandr Nikolich, Vladimir Arkhipkin, Igor Pavlov, Andrey Kuznetsov, and Denis Dimitrov. kandinsky 2.2, 2023. 13
- [70] Jascha Sohl-Dickstein, Eric Weiss, Niru Maheswaranathan, and Surya Ganguli. Deep unsupervised learning using nonequilibrium thermodynamics. In *International conference on machine learning*, pages 2256–2265. pmlr, 2015. 1
- [71] Michael Soloveitchik, Tzvi Diskin, Efrat Morin, and Ami Wiesel. Conditional frechet inception distance. *arXiv preprint arXiv:2103.11521*, 2021. 2, 4, 8
- [72] George Stein, Jesse Cresswell, Rasa Hosseinzadeh, Yi Sui, Brendan Ross, Valentin Vilecroze, Zhaoyan Liu, Anthony L Caterini, Eric Taylor, and Gabriel Loaiza-Ganem. Exposing flaws of generative model evaluation metrics and their

- unfair treatment of diffusion models. *Advances in Neural Information Processing Systems*, 36:3732–3784, 2023. 2, 4, 5
- [73] Andreas Steiner, Alexander Kolesnikov, Xiaohua Zhai, Ross Wightman, Jakob Uszkoreit, and Lucas Beyer. How to train your vit? data, augmentation, and regularization in vision transformers. *arXiv preprint arXiv:2106.10270*, 2021. 12
- [74] Christian Szegedy, Vincent Vanhoucke, Sergey Ioffe, Jon Shlens, and Zbigniew Wojna. Rethinking the inception architecture for computer vision. In *Proceedings of the IEEE conference on computer vision and pattern recognition*, pages 2818–2826, 2016. 2, 8, 12
- [75] Thomas Unterthiner, Sjoerd Van Steenkiste, Karol Kurach, Raphaël Marinier, Marcin Michalski, and Sylvain Gelly. Fvd: A new metric for video generation. 2019. 4
- [76] Lokesh Veeramacheni, Moritz Wolter, Hildegard Kuehne, and Juergen Gall. Fr\`echet wavelet distance: A domain-agnostic metric for image generation. *arXiv preprint arXiv:2312.15289*, 2023. 2
- [77] Benjamin Warner, Antoine Chaffin, Benjamin Clavié, Orion Weller, Oskar Hallström, Said Taghadouini, Alexis Gallagher, Raja Biswas, Faisal Ladhak, Tom Aarsen, et al. Smarter, better, faster, longer: A modern bidirectional encoder for fast, memory efficient, and long context finetuning and inference. *arXiv preprint arXiv:2412.13663*, 2024. 12
- [78] Xiaoshi Wu, Yiming Hao, Keqiang Sun, Yixiong Chen, Feng Zhu, Rui Zhao, and Hongsheng Li. Human preference score v2: A solid benchmark for evaluating human preferences of text-to-image synthesis. *arXiv preprint arXiv:2306.09341*, 2023. 2, 3, 4, 5
- [79] Xiaoshi Wu, Keqiang Sun, Feng Zhu, Rui Zhao, and Hongsheng Li. Human preference score: Better aligning text-to-image models with human preference. In *Proceedings of the IEEE/CVF International Conference on Computer Vision*, pages 2096–2105, 2023. 1, 2, 6
- [80] Hu Xu, Saining Xie, Xiaoqing Ellen Tan, Po-Yao Huang, Russell Howes, Vasu Sharma, Shang-Wen Li, Gargi Ghosh, Luke Zettlemoyer, and Christoph Feichtenhofer. Demystifying clip data. *arXiv preprint arXiv:2309.16671*, 2023. 8, 12
- [81] Jiazheng Xu, Xiao Liu, Yuchen Wu, Yuxuan Tong, Qinkai Li, Ming Ding, Jie Tang, and Yuxiao Dong. Imagereward: Learning and evaluating human preferences for text-to-image generation. *Advances in Neural Information Processing Systems*, 36:15903–15935, 2023. 1, 2, 3, 5
- [82] Tao Xu, Pengchuan Zhang, Qiuyuan Huang, Han Zhang, Zhe Gan, Xiaolei Huang, and Xiaodong He. Attngan: Fine-grained text to image generation with attentional generative adversarial networks. In *Proceedings of the IEEE conference on computer vision and pattern recognition*, pages 1316–1324, 2018. 2
- [83] Zhuoyi Yang, Jiayan Teng, Wendi Zheng, Ming Ding, Shiyu Huang, Jiazheng Xu, Yuanming Yang, Wenyi Hong, Xiaohan Zhang, Guanyu Feng, et al. Cogvideox: Text-to-video diffusion models with an expert transformer. *arXiv preprint arXiv:2408.06072*, 2024. 1
- [84] Jiahui Yu, Yuanzhong Xu, Jing Yu Koh, Thang Luong, Gunjan Baid, Zirui Wang, Vijay Vasudevan, Alexander Ku, Yinfei Yang, Burcu Karagol Ayan, et al. Scaling autoregressive models for content-rich text-to-image generation. *arXiv preprint arXiv:2206.10789*, 2(3):5, 2022. 2
- [85] Xiaohua Zhai, Basil Mustafa, Alexander Kolesnikov, and Lucas Beyer. Sigmoid loss for language image pre-training. In *Proceedings of the IEEE/CVF international conference on computer vision*, pages 11975–11986, 2023. 12
- [86] Han Zhang, Tao Xu, Hongsheng Li, Shaoting Zhang, Xiaogang Wang, Xiaolei Huang, and Dimitris N Metaxas. Stackgan: Text to photo-realistic image synthesis with stacked generative adversarial networks. In *Proceedings of the IEEE international conference on computer vision*, pages 5907–5915, 2017. 2
- [87] Lvmin Zhang, Anyi Rao, and Maneesh Agrawala. Adding conditional control to text-to-image diffusion models. In *Proceedings of the IEEE/CVF international conference on computer vision*, pages 3836–3847, 2023. 1, 8
- [88] Richard Zhang, Phillip Isola, Alexei A Efros, Eli Shechtman, and Oliver Wang. The unreasonable effectiveness of deep features as a perceptual metric. In *Proceedings of the IEEE conference on computer vision and pattern recognition*, pages 586–595, 2018. 2
- [89] Sixian Zhang, Bohan Wang, Junqiang Wu, Yan Li, Tingting Gao, Di Zhang, and Zhongyuan Wang. Learning multi-dimensional human preference for text-to-image generation. In *Proceedings of the IEEE/CVF Conference on Computer Vision and Pattern Recognition*, pages 8018–8027, 2024. 2, 3, 5
- [90] Sixian Zhang, Bohan Wang, Junqiang Wu, Yan Li, Tingting Gao, Di Zhang, and Zhongyuan Wang. Learning multi-dimensional human preference for text-to-image generation. In *Proceedings of the IEEE/CVF Conference on Computer Vision and Pattern Recognition*, pages 8018–8027, 2024. 2
- [91] Yufan Zhou, Ruiyi Zhang, Changyou Chen, Chunyuan Li, Chris Tensmeyer, Tong Yu, Jiuxiang Gu, Jinhui Xu, and Tong Sun. Towards language-free training for text-to-image generation. In *Proceedings of the IEEE/CVF conference on computer vision and pattern recognition*, pages 17907–17917, 2022. 13

A. Image and Text Backbone Models

In our experiments, we used 46 different image backbone models and 43 different text backbone models. For vision models, we employed those trained with self-supervised learning, including ViT trained on ImageNet-1k [15], ViT trained on ImageNet-21k [73], MAE [28], DINOv2 [55], MoCOv3 [7], and I-JEPA trained on both ImageNet-1k and ImageNet-22k [3]. We also incorporated image-and-text-aligned pretrained models such as CLIP [59], MetaCLIP [80], DFN-CLIP [19], OpenCLIP [9], DataComp-CLIP [22], ConvNeXT-CLIP [67], EVA02 [20], and SigLIP [85]. Additional image models included SAM-ViT [35] and Inception V3 [74]. For text models, we employed autoencoding models such as RoBERTa [49], BERT [13], ALBERT [42], ModernBERT [77], XLM-RoBERTa [12], as well as sequence-to-sequence models

Models	Statistical Metric										Human Preference Trained Metric									
	Human \uparrow		FID \downarrow		FD _{DINOv2} \downarrow		CLIP \uparrow		CMMD \downarrow		cFreD \downarrow		Aesthetic \uparrow		ImReward \uparrow		HPS v2 \uparrow		MPS \uparrow	
	R#	Rate	R#	Score	R#	Score	R#	Score	R#	Score	R#	Score	R#	Score	R#	Score	R#	Score	R#	Score
<i>GLIDE</i> [53]	1	80.87%	1	7.90	1	6.88	9	14.34	1	2.42	1	3.79	1	5.55	3	0.37	2	25.52	1	12.72
<i>COCO</i> [45]	2	80.66%	7	13.11	7	13.05	10	13.11	5	15.07	4	4.55	5	5.03	1	0.55	1	25.64	5	10.92
<i>FuseDream</i> [48]	3	76.29%	2	8.39	2	7.59	5	15.07	4	5.41	2	4.16	4	5.34	2	0.47	3	24.40	2	12.44
<i>DALLE 2</i> [62]	4	75.87%	3	9.16	3	7.95	8	14.39	3	4.06	3	4.42	3	5.40	6	0.07	5	23.81	4	11.75
<i>VQGAN+CLIP</i> [17]	5	68.78%	4	10.11	4	8.70	7	14.41	2	3.70	5	4.90	2	5.40	5	0.08	4	23.93	3	11.82
<i>CogView2</i> [14]	6	39.00%	6	12.65	6	12.87	3	15.45	8	45.64	7	6.93	7	4.82	7	0.02	7	19.45	7	8.85
<i>SDv1.4</i> [63]	7	38.36%	5	12.51	5	11.93	4	15.42	6	28.52	8	7.18	8	4.56	8	-0.67	8	19.44	8	8.00
<i>VQ-Diffusion</i> [24]	8	32.04%	8	13.85	8	13.12	6	14.71	7	33.40	6	6.59	6	4.88	4	0.17	6	21.91	6	10.15
<i>SDv2.0</i> [63]	9	22.00%	9	14.74	9	14.23	2	15.62	10	55.88	9	8.16	9	4.54	9	-0.72	9	18.45	9	7.24
<i>LAFITE</i> [91]	10	9.07%	10	15.12	10	14.63	1	16.01	9	53.22	10	9.06	10	4.23	10	-1.45	10	15.03	10	5.08
ρ^2	-	-	1	0.70	1	0.65	1	0.63	1	0.88	0.97	-	0.83	-	0.71	-	<u>0.90</u>	-	0.86	-
Rank Acc.	-	-	1	86.7	1	86.7	1	15.6	1	80.0	91.1	-	82.2	-	84.4	-	<u>88.9</u>	-	86.7	-

Table B.1. Text-to-image model ranking and scores by statistical models (FID, FD_{DINOv2}, CLIP score, CMMD, and cFreD) and models that were trained with human preference (Aesthetic Score, ImageReward, HPSv2, and MPS) on HPDv2 test set. Best results in **bold**, second best underlined

Models	Statistical Metric										Human Preference Trained Metric									
	Human \uparrow		FID \downarrow		FD _{DINOv2} \downarrow		CLIP \uparrow		CMMD \downarrow		cFreD \downarrow		Aesthetic \uparrow		ImReward \uparrow		HPS v2 \uparrow		MPS \uparrow	
	R#	Rate	R#	Score	R#	Score	R#	Score	R#	Score	R#	Score	R#	Score	R#	Score	R#	Score	R#	Score
<i>SDXL</i> [58]	1	69.84%	1	31.24	1	23.50	2	32.79	1	2.55	1	2.98	3	5.64	1	0.95	1	28.63	4	10.33
<i>Kand2</i> [69]	2	46.10%	2	32.08	2	24.35	3	32.62	2	2.77	2	3.21	2	5.65	2	0.90	2	28.13	2	11.29
<i>Wuerst</i> [57]	3	42.68%	3	38.43	3	30.93	4	31.72	3	3.83	3	4.18	1	5.71	3	0.79	3	27.79	1	11.30
<i>Karlo</i> [43]	4	29.21%	4	48.40	4	41.57	1	33.01	4	19.95	4	5.45	4	4.93	4	0.70	4	26.56	3	11.11
ρ^2	-	-	1	0.70	1	0.70	1	0.12	1	0.54	1	0.73	1	0.43	-	<u>0.81</u>	-	0.83	-	0.65

Table B.2. Text-to-image model ranking and scores by statistical metrics (FID, FD_{DINOv2}, CLIP score, CMMD, and cFreD) and models that were trained with human preference (Aesthetic Score, ImageReward, and MPS) on Parti-Prompt. Best results in **bold**, second best underlined

including FLAN-T5 [11] and T5 [60] were used. We also used the text encoders from the aforementioned image-and-text-aligned pretrained models. The complete lists of image and text backbone models used in our experiments are presented in Tables C.1 and C.2, respectively.

B. Results on Text-to-Image

We provide in-depth results on three text-to-image benchmarks: HPDv2 (Tab. B.1), Parti-Prompts (Tab. B.2), and a random selection of COCO prompts (Tab. B.3).

Results on HPDv2. Table B.1 summarizes the rankings and scores for images generated by various models—including one real image—across multiple evaluation metrics. Notably, cFreD achieves the highest alignment with human preferences, reaching a correlation of 0.97. Among statistical metrics, cFreD attains the highest correlation and is comparable to HPSv2 (0.94), a model explicitly trained on

human preferences. Given that HPSv2 was trained on the HPSv2 training set, which includes four models from the test set, and employed the same annotators, it inherently encodes specific human preference biases of the same setting. In contrast, cFreD achieves comparable or superior correlation with human evaluation without any human preference training. These results demonstrate that cFreD provides more reliable rankings across diverse models compared to standard automatic metrics and metrics trained explicitly on human preference data.

Table B.1 also reports the rank accuracy scores on the HPDv2 test set. Among all evaluated metrics, cFreD achieves the highest rank accuracy (91.1%), highlighting its strong correspondence with human judgments. HPSv2 follows as the second-best metric with an accuracy of 88.9%, while both FID and FD_{DINOv2} obtain competitive scores of 86.7%. Overall, although models trained with human preference data tend

Models	Statistical Metric										Human Preference Trained Metric									
	Humans \uparrow		FID \downarrow		FD _{DINOv2} \downarrow		CLIP \uparrow		CMMD \downarrow		cFreD \downarrow		Aesthetic \uparrow		ImReward \uparrow		HPS v2 \uparrow		MPS \uparrow	
	R#	ELO	R#	Score	R#	Score	R#	Score	R#	Score	R#	Score	R#	Score	R#	Score	R#	Score	R#	Score
<i>FLUX.1[dev]</i> [41]	1	1083	5	10.45	7	7.21	9	30.72	8	6.08	4	9.93	2	5.75	3	1.10	2	30.74	2	12.90
<i>SDv3.5-L Turbo</i> [18]	2	1073	9	11.68	9	8.12	6	31.11	7	48.52	7	10.44	6	5.50	6	0.64	7	26.52	6	10.88
<i>SDv3.5-L</i> [18]	3	1069	2	10.27	4	6.77	1	31.74	4	40.27	2	9.49	4	5.55	2	1.10	3	30.07	3	12.30
<i>Playgroundv2.5</i> [44]	4	997	7	10.90	8	7.50	7	31.03	9	66.10	5	10.08	1	6.16	1	1.15	1	31.56	1	13.15
<i>SDv3-M</i> [18]	5	944	6	10.46	5	7.09	3	31.68	2	34.34	1	9.49	7	5.45	4	1.08	4	29.80	9	2.35
<i>SDXL</i> [58]	6	890	3	10.31	2	6.66	2	31.70	6	45.07	3	9.73	3	5.61	5	0.76	5	28.34	4	12.08
<i>SDv2.1</i> [63]	7	752	1	10.14	1	6.55	4	31.42	3	35.17	6	10.24	5	5.52	8	0.41	6	26.58	5	10.90
<i>Janus Pro</i> [8]	8	740	8	10.97	6	7.17	8	30.99	5	43.51	9	10.76	9	5.33	7	0.57	8	26.22	7	10.70
<i>SDv1.5</i> [63]	9	664	4	10.41	3	6.73	5	31.21	1	29.89	8	10.58	8	5.34	9	0.19	9	26.15	8	10.50
ρ^2	-		0.08		0.29		0.00		0.22		0.33		0.27		0.69		0.48		0.48	
Rank Acc.	-		41.67		36.11		47.22		30.56		66.67		<u>72.22</u>		80.56		80.56		80.56	

Table B.3. Text-to-image model ranking by automatic models(FID, FD_{DINOv2}, CLIP score, CMMD, and cFreD) and models that were trained with human preference (Aesthetic Score, ImageReward, HPSv2, and MPS) on randomly sampled COCO prompts. Rank Acc. below 0.5 indicates there are more discordant pairs than concordant ones. Best results in **bold**, second best underlined

to align well with human judgments, cFreD emerges as the most robust and reliable metric.

Result on PartiPrompts Arena. Table B.2 presents the rankings and scores of text-to-image models evaluated on the Parti-Prompt Arena using both statistical metrics and human preference-trained models. Among the statistical metrics, cFreD achieves the highest correlation with human evaluations (0.73), with FID and FD_{DINOv2} both reaching a correlation of 0.70. In contrast, the CLIP score shows a very low correlation (0.12) with human judgments. In the human preference trained category, HPSv2 has the strongest alignment, achieving the highest correlation (0.83), followed by ImageReward (0.81) and MPS (0.65). These results highlight that while cFreD is a robust automatic metric, HPSv2 stands out as the most effective in capturing human evaluation trends in the PartiPrompts Arena.

Results on COCO. Table B.3 presents an evaluation on the COCO dataset using nine modern text-to-image models, with human preference rankings sourced from the Text-to-Image Leaderboard and expressed as ELO scores. Among statistical metrics (FID, FD_{DINOv2}, CLIP, CMMD, and our proposed cFreD), only cFreD exhibits a strong correlation with human preferences, achieving a correlation of 0.33 and a non-trivial rank accuracy of 66.67%. This result places cFreD as the third most aligned metric overall, surpassed only by the human preference-trained metrics ImageReward, HPSv2, and MPS. Notably, all other statistical metrics show considerably weaker alignment with ELO rankings and, as a result, inverted the rankings, resulting in a Rank Acc. below 0.5. These findings highlight that cFreD is sensitive to both visual fidelity and prompt consistency, reinforcing its value as a practical, training-free alternative for benchmarking

text-to-image generation.

C. Analysis on Selecting Image and Text Backbone Models

We provide an in-depth analysis of how different image and text models affect cFreD. In our experiments, we tested all possible combinations of 43 different image and text models, focusing exclusively on ViT-based architectures and excluding SigLIP models with high-resolution options.

C.1. Spearman Correlation

We present Spearman correlation heatmaps that compare various text and image models across three distinct datasets: Parti-Prompts, HPDv2, and a random selection of COCO prompts.

Fig. C.1 showcases the heatmap on Parti-Prompts. Notably, certain image models such as ViT-B/16 trained on ImageNet-1K and ViT-H/14 trained on ImageNet-21K show consistently high performance with different text models. In contrast, SAM-ViT-H/16 presents more variability with different text models. While most ViT, DINO, and CLIP-based models demonstrate strong correlations across different text models, MAE models show slightly lower correlations.

Fig. C.2 presents the heatmap on HPDv2. Most models show strong correlations, whereas MAE models and SAM have lower correlations. Regardless of their performance levels, all image models show consistent correlation patterns across different text models.

Fig. C.3 provides the heatmap on randomly selected COCO prompts. The correlation values are significantly lower overall, ranging from approximately 0.00 to 0.30, which is much lower than both the Parti-Prompts and HPDv2

datasets. Most models show lower correlations, while only DINOv2 models consistently demonstrate stronger correlations. Compared to other datasets, this heatmap exhibits more variability, such as OpenCLIP showing a mixture of relatively higher and lower correlations depending on the text models.

These results highlight the importance of selecting compatible text and image models for improved cross-modal understanding, as not all combinations yield equally robust alignment. Additionally, it suggests that selecting a suitable image encoder plays a more pivotal role than choosing a text encoder, indicating that image encoder choice exerts a greater influence on overall performance.

C.2. Effect of Visual Encoders on HPDv2

In this section, we provide an analysis of how different visual encoder characteristics impact cFreD’s correlation with human preferences on HPDv2. For each factor examined, we report the average correlation across all possible text encoder combinations.

Effect of the size of the pre-training dataset on cFreD. Fig. C.4a shows the correlation between cFreD and human preferences as a function of the size of the pre-training dataset for Vision Transformer (ViT). In all ranges, it shows high alignment with human judgments, with a correlation higher than 0.95 across all data sizes. This indicates that factors beyond raw data quantity, such as diversity and quality, significantly influence performance.

Effect of image size on cFreD. Fig. C.4b illustrates the correlation between cFreD and human preferences across varying input image resolutions. We observe a nonmonotonic relationship: increasing resolutions do not consistently yield higher correlations. In particular, an image size from 224x224 to 896x896 all achieves a high correlation above 0.96. However, beyond 518x518, performance declines, reaching 0.964 at 896x896 and showing the lowest correlation of 0.774 at 1024x1024.

Effect of ViT model size on cFreD. The correlation between cFreD and human preferences across Vision Transformer (ViT) sizes are presented in Fig. C.4c. It shows that all models achieve consistently high correlations—ranging from 0.945 to 0.986—indicating strong agreement with the target metric across scales. Interestingly, the *SO* model attains the highest correlation at 0.986, while *Gigantic* has the lowest, though still robust correlation of 0.945. The remaining models also cluster around correlations between 0.96 and 0.98, suggesting that simply increasing model size does not guarantee a strictly monotonic improvement in correlation.

Effect of ViT Feature dimensionality on cFreD. Fig. C.4d shows the correlation between cFreD and human preferences across ViT feature dimensions from 256 to 1664. The lowest number of the feature (256) shows the lowest correlation. However, we observe a clear plateau effect in performance

once the feature count reaches 384, with correlation values stabilizing around 0.98-0.99 across a wide range of dimensionalities (512-1408). Interestingly, at extremely high dimensionalities (above 1536), we note a slight performance decline, with correlation dropping to 0.95 at 1664 features. This suggests an optimal range for feature dimensionality exists, beyond which additional computational complexity yields diminishing or even negative returns.

Effect of Zero-Shot ImageNet Accuracy on cFreD. Fig. C.4e depicts a boxplot of the correlation between cFreD and human preferences as a function of zero-shot ImageNet accuracy, evaluated exclusively on image-text pretrained models [59]. Higher zero-shot accuracies generally correspond to stronger correlations with human judgments, though variance exists within each accuracy bin. Interestingly, we find that correlations peak at a model with 66.58% zero-shot accuracy and decrease as model accuracy gets higher.

C.3. Effect of Visual Encoders on COCO prompts

In this section, we provide an analysis of how different visual encoder characteristics impact cFreD’s correlation with human preferences on randomly selected COCO prompts. For each factor examined, we report the average correlation across all possible text encoder combinations.

Effect of the size of the pre-training dataset on cFreD. Fig. C.5a illustrates the correlation between cFreD and human preferences as a function of the pre-training dataset size for Vision Transformer (ViT). We observe a nonmonotonic relationship: increasing the pre-training dataset size does not consistently yield higher correlations. Notably, a model trained with fewer than 100 million samples achieves a high correlation of 0.33, while models trained with larger datasets show lower correlations ranging from 0.06 to 0.21. Interestingly, models trained with fewer than 5 billion samples demonstrate the lowest human correlation (0.06). These findings indicate that simply scaling up data does not guarantee improved performance for every metric or task, suggesting that balancing the quantity and quality of training data is crucial for optimal results.

Effect of image size on cFreD. Fig. C.4b illustrates the correlation between cFreD and human preferences across varying input image resolutions. We observe an inconsistent relationship: starting around 0.05 at an image size of 224x224, then rising to about 0.10 at 256x256 before dropping again to around 0.03 at 299x229. After a modest increase to 0.08 at 384x384, the correlation dips to 0.01 at 448x448 and then peaks sharply at 0.18 for an image size of 518x518. Beyond that, it decreases to nearly 0 at 896x896 and recovers slightly to 0.03 at 1024. These erratic trends suggest that there is no straightforward, monotonic relationship between image size and correlation for this particular task or metric, and the highest correlation appears in the

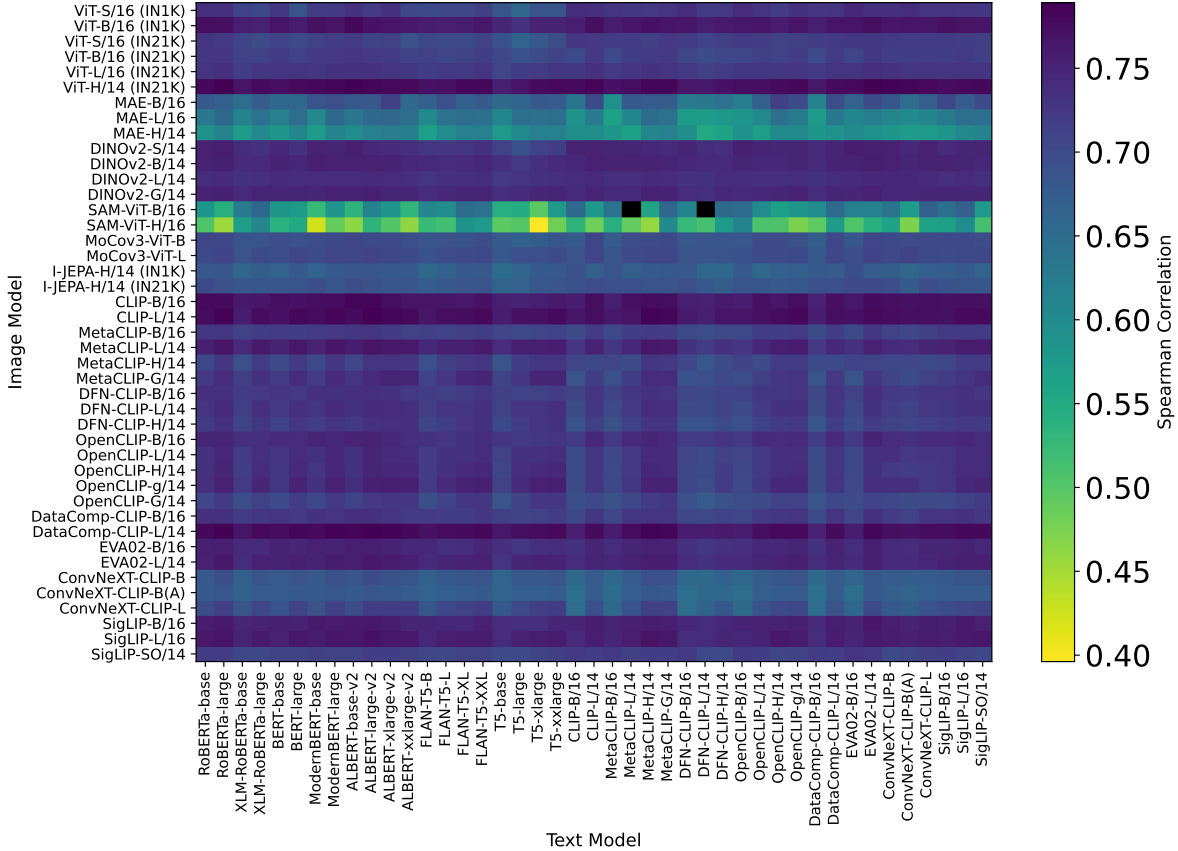


Figure C.1. Spearman Correlation Heatmap on Parti-Prompts.

midrange rather than at the smallest or largest resolutions.

Effect of ViT model size on cFreD. The correlation between cFreD and human preferences across Vision Transformer (ViT) sizes are presented in Fig. C.4c. Larger models tend to improve alignment with human judgments, with *Giant* model achieving the highest correlation of 0.320. However, when the model size gets bigger to *Gigantic* model, the correlation degrades down to 0.089. These results indicate that correlation does not simply increase in tandem with model size; rather, there seems to be an optimal range, as exemplified by the *Giant* model, for achieving the strongest alignment with the evaluation metric.

Effect of ViT Feature dimensionality on cFreD. Fig. C.4d shows the correlation between cFreD and human preferences across ViT feature dimensions from 256 to 1664. The two lowest numbers of the features (256 and 384) show the lowest correlation. However, we observe a clear plateau effect in performance once the feature count reaches 512, with correlation values stabilizing around 0.30-0.32 across a wide range of dimensionalities (512-1152). Interestingly, at extremely high dimensionalities (above 1536), we note a slight performance decline, with correlation dropping to 0 at the 1408 feature. Although the correlation increases

back to 0.32 with 1536 features, it decreases back to 0.14 at 1664 features. This suggests an optimal range for feature dimensionality exists, beyond which additional computational complexity yields diminishing or even negative returns.

Effect of Zero-Shot ImageNet Accuracy on cFreD. Fig. C.4e depicts a boxplot of the correlation between cFreD and human preferences as a function of zero-shot ImageNet accuracy, evaluated exclusively on image-text pretrained models [59]. Interestingly, we find that the lowest zero-shot accuracy has the highest correlation to human preference. However, after 68.58 of zero-shot accuracies, higher zero-shot accuracies generally correspond to stronger correlations with human judgments, though variance exists within each accuracy bin.

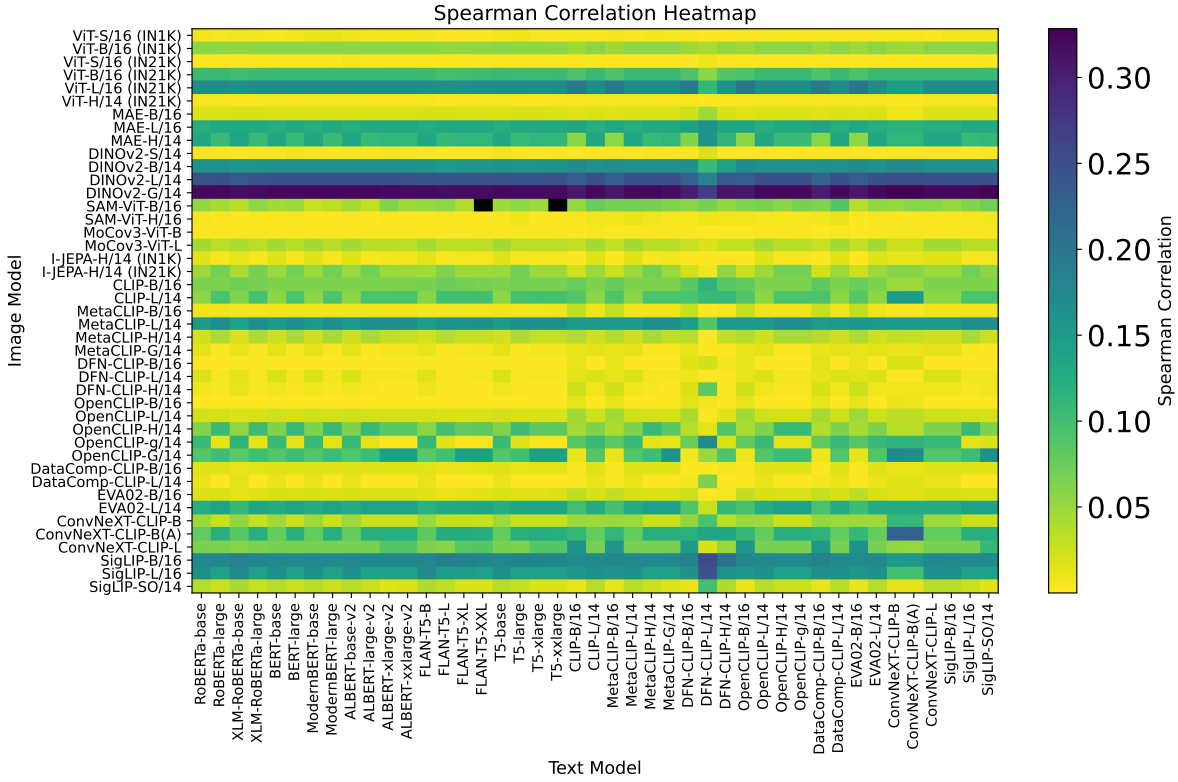


Figure C.3. Spearman Correlation Heatmap on random COCO prompts.

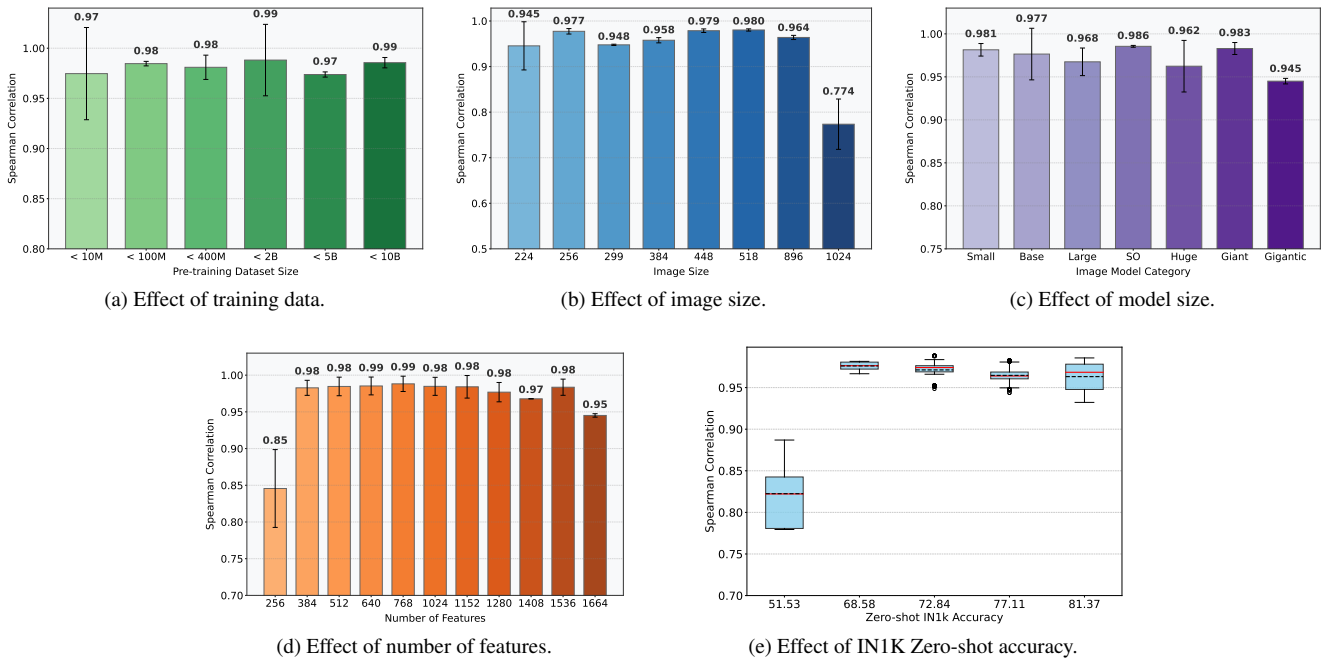
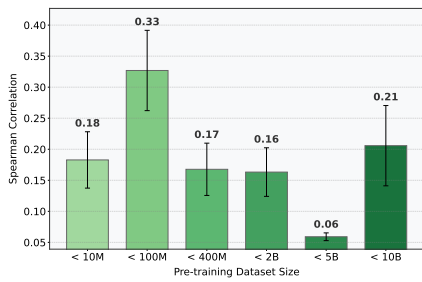
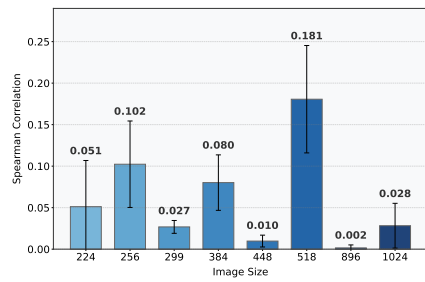


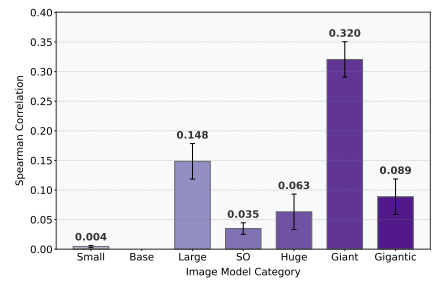
Figure C.4. Ablation study on the HPDv2 dataset comparing the correlation to human preferences under varying factors: (a) the ViT training dataset, (b) input image size, (c) model capacity, (d) the number of features in the last ViT layer, and (e) zero-shot accuracy on ImageNet-1K.



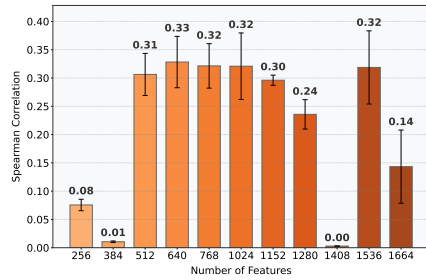
(a) Effect of training data.



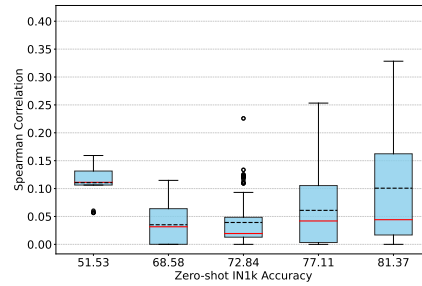
(b) Effect of image size.



(c) Effect of model size.



(d) Effect of number of features.



(e) Effect of IN1K Zero-shot accuracy.

Figure C.5. **Ablation study on randomly sampled COCO prompts** comparing the correlation to human preferences under varying factors: (a) the ViT training dataset, (b) input image size, (c) model capacity, (d) the number of features in the last ViT layer, and (e) zero-shot accuracy on ImageNet-1K.

Model Name	Model Path
ViT-S/16 (IN1K)	timm/vit_small_patch16_224.augreg_in1k
ViT-B/16 (IN1K)	timm/vit_base_patch16_224.augreg_in1k
ViT-S/16 (IN21K)	timm/vit_small_patch16_224.augreg_in21k
ViT-B/16 (IN21K)	timm/vit_base_patch16_224.augreg_in21k
ViT-L/16 (IN21K)	timm/vit_large_patch16_224.augreg_in21k
ViT-H/14 (IN21K)	timm/vit_huge_patch14_224.orig_in21k
MAE-B/16	timm/vit_base_patch16_224.mae
MAE-L/16	timm/vit_large_patch16_224.mae
MAE-H/14	timm/vit_huge_patch14_224.mae
DINOv2-S/14	timm/vit_small_patch14_dinov2.lvd142m
DINOv2-B/14	timm/vit_base_patch14_reg4_dinov2.lvd142m
DINOv2-L/14	timm/vit_large_patch14_dinov2.lvd142m
DINOv2-G/14	timm/vit_giant_patch14_dinov2.lvd142m
SAM-ViT-B/16	timm/samvit_base_patch16
SAM-ViT-H/16	timm/samvit_huge_patch16
MoCov3-ViT-B	nyu-visionx/moco-v3-vit-b
MoCov3-ViT-L	nyu-visionx/moco-v3-vit-l
I-JEPA-H/14 (IN1K)	jmtzt/ijepa_vith14_1k
I-JEPA-H/14 (IN21K)	facebook/ijepa_vith14_22k
CLIP-B/16	timm/vit_base_patch16_clip_224.openai
CLIP-L/14	timm/vit_large_patch14_clip_224.openai
MetaCLIP-B/16	timm/vit_base_patch16_clip_224.metaclip_400m
MetaCLIP-L/14	timm/vit_large_patch14_clip_224.metaclip_400m
MetaCLIP-H/14	timm/vit_huge_patch14_clip_224.metaclip_altogether
MetaCLIP-G/14	timm/vit_gigantic_patch14_clip_224.metaclip_2pt5b
DFN-CLIP-B/16	timm/vit_base_patch16_clip_224.dfn2b
DFN-CLIP-L/14	timm/vit_large_patch14_clip_224.dfn2b
DFN-CLIP-H/14	timm/vit_huge_patch14_clip_224.dfn5b
OpenCLIP-B/16	timm/vit_base_patch16_clip_224.laion2b
OpenCLIP-L/14	timm/vit_large_patch14_clip_224.laion2b
OpenCLIP-H/14	timm/vit_huge_patch14_clip_224.laion2b
OpenCLIP-g/14	timm/vit_giant_patch14_clip_224.laion2b
OpenCLIP-G/14	timm/vit_gigantic_patch14_clip_224.laion2b
DataComp-CLIP-B/16	timm/vit_base_patch16_clip_224.datacomp1
DataComp-CLIP-L/14	timm/vit_large_patch14_clip_224.datacomp1
EVA02-B/16	timm/eva02_base_patch16_clip_224
EVA02-L/14	timm/eva02_large_patch14_clip_224
ConvNeXT-CLIP-B	timm/convnext_base_clip_laion2b
ConvNeXT-CLIP-B(A)	timm/convnext_base_clip_laiona
ConvNeXT-CLIP-L	timm/convnext_large_mlp_clip_laion2b.augreg
SigLIP-B/16	timm/vit_base_patch16_siglip_224.webli
SigLIP-L/16	timm/vit_large_patch16_siglip_256.webli
SigLIP-SO/14	timm/vit_so400m_patch14_siglip_gap_224.webli
InceptionV3	inception/inceptionv3
SigLIP-SO/14 (448)	timm/vit_so400m_patch14_siglip_gap_448.pali2_10b_pt
SigLIP-SO/14 (896)	timm/vit_so400m_patch14_siglip_gap_896.pali2_10b_pt

Table C.1. List of image backbone models used in our analysis.

Model Name	Model Path
RoBERTa-base	FacebookAI/roberta-base
RoBERTa-large	FacebookAI/roberta-large
XLNet-base	FacebookAI/xlnet-base
XLNet-large	FacebookAI/xlnet-large
BERT-base	google-bert/bert-base-uncased
BERT-large	google-bert/bert-large-uncased
ModernBERT-base	answerdotai/ModernBERT-base
ModernBERT-large	answerdotai/ModernBERT-large
ALBERT-base-v2	albert/albert-base-v2
ALBERT-large-v2	albert/albert-large-v2
ALBERT-xlarge-v2	albert/albert-xlarge-v2
ALBERT-xxlarge-v2	albert/albert-xxlarge-v2
FLAN-T5-B	google/flan-t5-base
FLAN-T5-L	google/flan-t5-large
FLAN-T5-XL	google/flan-t5-xl
FLAN-T5-XXL	google/flan-t5-xxl
T5-base	google/t5-v1.1-base
T5-large	google/t5-v1.1-large
T5-xlarge	google/t5-v1.1-xl
T5-xxlarge	google/t5-v1.1-xxl
CLIP-B/16	ViT-B-16-quickgelu.openai
CLIP-L/14	ViT-L-14-quickgelu.openai
MetaCLIP-B/16	ViT-B-16-quickgelu.metaclip_400m
MetaCLIP-L/14	ViT-L-14-quickgelu.metaclip_400m
MetaCLIP-H/14	ViT-H-14.metaclip_altogether
MetaCLIP-G/14	ViT-bigG-14-CLIPA.datacomp1b
DFN-CLIP-B/16	ViT-B-16-quickgelu.dfn2b
DFN-CLIP-L/14	ViT-L-14-quickgelu.dfn2b
DFN-CLIP-H/14	ViT-H-14-quickgelu.dfn5b
OpenCLIP-B/16	ViT-B-16.laion2b_s34b_b88k
OpenCLIP-L/14	ViT-L-14.laion2b_s32b_b82k
OpenCLIP-H/14	ViT-H-14.laion2b_s32b_b79k
OpenCLIP-g/14	ViT-g-14.laion2b_s34b_b88k
DataComp-CLIP-B/16	ViT-B-16.datacomp_xl_s13b_b90k
DataComp-CLIP-L/14	ViT-L-14.datacomp_xl_s13b_b90k
EVA02-B/16	EVA02-B-16.merged2b_s8b_b131k
EVA02-L/14	EVA02-L-14.merged2b_s4b_b131k
ConvNeXT-CLIP-B	convnext_base_w.laion2b_s13b_b82k_augreg
ConvNeXT-CLIP-B(A)	convnext_base_w.laion_aesthetic_s13b_b82k
ConvNeXT-CLIP-L	convnext_large_d.laion2b_s26b_b102k_augreg
SigLIP-B/16	ViT-B-16-SigLIP.webli
SigLIP-L/16	ViT-L-16-SigLIP-256.webli
SigLIP-SO/14	ViT-SO400M-14-SigLIP.webli

Table C.2. List of text backbone models used in our analysis.